

Stable, tunable calibration source for large-beam optical systems

Todd G. Ulmer, Amy C. Raudenbush, and Vicky Loriaux

An optical calibration source for free-space systems with large beams is presented. It produces a 2 W, 370 mm beam tunable from 1545–1570 nm with a wavefront error of $<\lambda/15$ peak to valley and $<0.013\lambda$ rms at 1550 nm, power stability of $<\pm 0.02$ dB, arbitrarily selected polarization, and polarization stability of $<\pm 1^\circ/\text{h}$ in orientation and $<\pm 0.02/\text{h}$ in ellipticity. © 2007 Optical Society of America

OCIS codes: 120.4640, 120.4820, 350.4800, 060.2310.

1. Introduction

Characterization of optical systems with beams larger than a few inches in diameter is hampered by many factors, including accumulated wavefront error, low power densities, and power instability introduced by atmospheric turbulence in the laboratory environment. Precise measurements require an optical reference source with pristine wavefront quality that is stable in both power and polarization so that any observed deviations from the ideal can be accurately ascribed to the system under test. Multiwatt powers are desirable for sufficient illumination of diagnostic sensors and for convenience in aligning large infrared beams. Furthermore, the generation of arbitrary polarization states is needed for assessment of polarization dependencies such as polarization-dependent loss. Finally, wavelength tunability is required for many applications.

In particular, large-beam systems incorporating a wavefront sensor can benefit from a stable, multiwatt optical source. Instruments for characterizing the wavefront error of an optical system can be divided into two categories: double pass (e.g., an interferometer) and single pass (e.g., a wavefront sensor). The geometry of many systems precludes the use of double-pass configurations; additionally, interferometric techniques can become problematic in systems with low power densities. The preferred solution for these applications is a single-pass configuration using a wave-

front sensor, which requires a stable optical source for the generation of reference files. Optical power is at a premium in large-beam systems where the wavefront sensor is a diagnostic tool tapped off the main signal path, and thus a stable, high-power, high-quality optical source is invaluable.

Here we present an optical calibration source that achieves the performance shown in Table 1. The calibration source is installed in a testbed in an optical testing facility that is used to characterize large optical systems. Measurements made with the calibration source require stability on the order of seconds to minutes; as will be shown in Section 3, this level of performance is readily achieved.

2. Method

A. Overview

The calibration source is shown in Fig. 1. To minimize the wavefront error, the approach taken is to limit the number of free-space components and to utilize fiber-optic components to implement the desired functionality, including laser amplification, heat-source remoting, alignment transfer, and polarization state generation. As shown in Fig. 1, light is launched from an angle-polished single-mode optical fiber, reflected by a single fold flat, and then collimated by an overfilled off-axis parabola (OAP) to create a quasi-Gaussian beam that is truncated at the 9% intensity point. In addition to providing a convenient optical point source, the fiber can be repositioned readily to allow access to a 633 nm Fizeau interferometer used for alignment of the OAP.

B. Fiber-Optic Components

The laser source is a master oscillator–power amplifier configuration. The master oscillator consists of a pair of sampled-grating distributed Bragg re-

The authors are with MIT Lincoln Laboratory, 244 Wood Street, Lexington, Massachusetts 02420, USA. T. Ulmer's e-mail address is ulmer@ll.mit.edu.

Received 31 July 2006; accepted 1 September 2006; posted 5 October 2006 (Doc. ID 73600); published 25 January 2007.

0003-6935/07/050669-07\$15.00/0

© 2007 Optical Society of America

Table 1. Calibration Source Performance

Parameter	Performance
Beam diameter	370 mm $1/e^2$ diameter, truncated at 406 mm
Wavelength range	1545–1570 nm
Wavefront error	$<\lambda/15$ peak to valley, 0.013λ rms at 1550 nm
Maximum power	>2 W
Power stability	$<\pm 0.02$ dB
Dynamic range	>20 dB
Polarization	arbitrary
Polarization stability	$<\pm 1^\circ/h$ in orientation $<\pm 0.02/h$ in ellipticity

flector (SG-DBR) tunable diode lasers¹ that together span the desired wavelength range, and the power amplifier is a dual-clad Er:Yb fiber amplifier. Although several individual tunable laser sources (e.g., external-cavity lasers) are available that would span the entire wavelength range, two factors led to the selection of the pair of SG-DBR lasers. First, the spare laser can serve as a holding beam to prevent dropouts in input power to the amplifier while the primary laser is being tuned to a new wavelength; thus, the amplifier can remain operational at nominal power during tuning to minimize thermal perturbations, enhancing power stability. Second, the relatively broad linewidth of the SG-DBR tunable diode lasers (5–10 MHz) helps minimize stimulated Brillouin scattering (SBS) in the fiber following the fiber amplifier. The reduced SBS allows remoting of the fiber components as far as several meters from the main free-space optical system to minimize air turbulence from heat sources such as the power amplifier. Traditional methods of SBS suppression such as current dithering or optical modulation were avoided here for reasons of stability and simplicity. Figure 2 shows an experimental comparison of the room-temperature SBS threshold in slow-axis-aligned PANDA polarization-maintaining fiber at 1559.8 nm for various commercial tunable laser sources; the SBS threshold for the SG-DBR laser is approximately

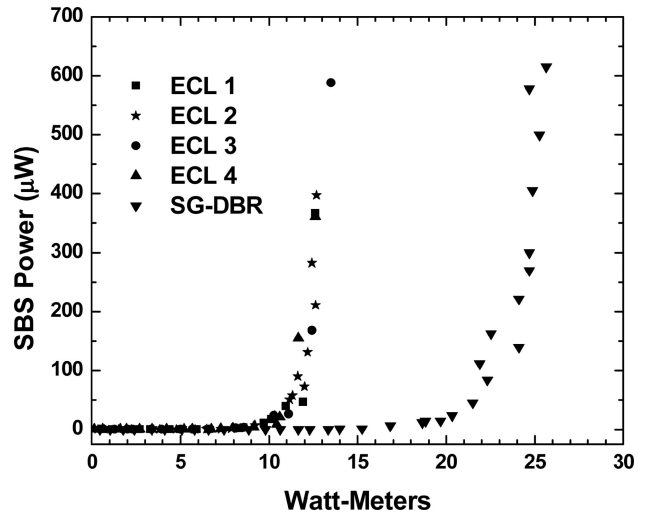


Fig. 2. SBS threshold at 1559.8 nm for various tunable laser sources in slow-axis-aligned PANDA fiber. ECL, external-cavity laser; SG-DBR, sampled-grating distributed Bragg reflector laser.

twice that of any of the four external-cavity lasers tested.

An active polarization controller based on a lithium niobate actuator^{2,3} is used to track out residual polarization fluctuations⁴ in the fiber amplifier, which is a dual-axis polarization-maintaining design. An error signal is derived from the second port of a high-power micro-optic polarization beam splitter (PBS). The error-signal power is scaled using two 1% fiber taps as attenuators, and an electrical error signal to drive the feedback circuit is generated using a 100 kHz photoreceiver. The PBS establishes a linear polarization with a polarization extinction ratio in excess of 25 dB as the input to the remainder of the calibration source, and the active polarization controller ensures that the power passing through the PBS is nominally as stable as the power generated directly by the fiber amplifier.

A high-power micro-optic circulator with polarization-maintaining pigtailed ports 1 and 2 transports a well-defined linear state of polarization to the

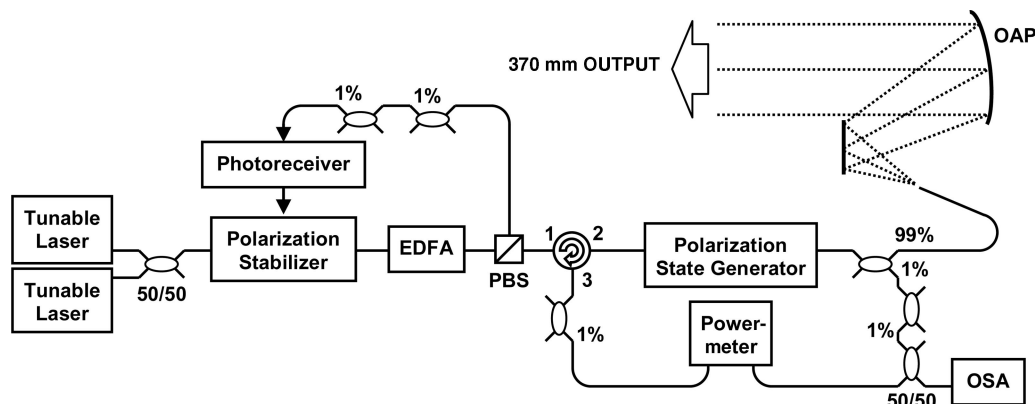


Fig. 1. Calibration source layout. OAP, off-axis parabola; EDFA, erbium-doped fiber amplifier; PBS, polarization beam splitter; OSA, optical spectrum analyzer.

non-polarization-maintaining input fiber of the second polarization controller, which functions as a polarization-state generator. The third port of the circulator provides a backreflection monitor path that is used for OAP alignment via a retroreflector; in addition, this path provides a means of monitoring for signs of SBS. The circulator also isolates the fiber amplifier from reflections.

The polarization-state generator is a fiber-squeezer design⁵ with minimal insertion loss, enabling high-power operation, and is used in conjunction with a polarimeter in the free-space optical testbed to adjust the polarization to any desired state. It is also capable of high-speed operation for applications that require polarization scrambling. The single-mode fiber on either side of the polarization controller is kept to a combined length of ~ 3 m and secured to minimize long-term polarization drift. The final components in the fiber-optic path are additional single-mode couplers to provide monitor points for outgoing power and wavelength.

The fiber-optic components are mounted on a $61\text{ cm} \times 92\text{ cm}$ aluminum plate. Other than securing components with standard screws and adhesive, no special precautions were necessary with respect to vibration or thermal isolation to achieve the stable performance described in Section 3. With the exception of the polarization controller fiber and the 1% tap

that follows, all components in the primary signal path are polarization maintaining.

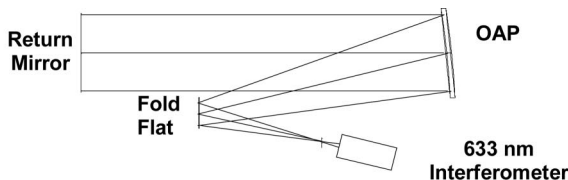
C. Free-Space Optics

The free-space optics consist of a high-quality fold flat and an OAP. The fold flat is a fused-silica substrate coated with protected silver to provide a surface figure of 0.048λ peak to valley and 0.008λ rms. The OAP is a Zerodur substrate coated with enhanced gold. The surface figure of the OAP, over a 419 mm clear aperture, is 0.050λ peak to valley and 0.006λ rms. The reflectance variation between vertical and horizontal polarization states is less than $\pm 0.1\%$ for each mirror, which is easily achieved because the angle of incidence on both mirrors is less than 20° .

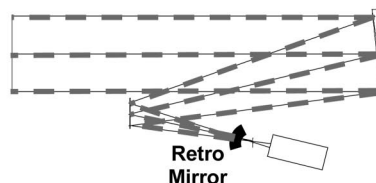
D. Alignment Procedure

The process used to align the calibration beam is shown in Fig. 3, and the associated alignment budgets for each step are shown in Table 2. Alignment of an OAP to an interferometer is a well-known procedure; the main challenge for creating a large collimated beam with the approach used here is transferring this alignment to the fiber source. This alignment transfer is accomplished using a spherical reference mirror to coalign the interferometer and the fiber. First, the 633 nm interferometer is aligned to the OAP so that

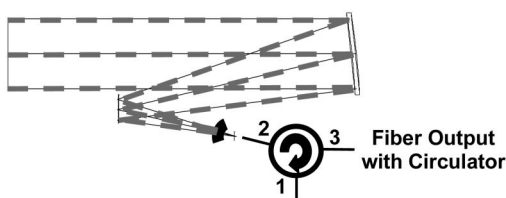
1. Align interferometer to off-axis parabola



2. Align interferometer to transfer mirror (reference sphere)



3. Align fiber to transfer mirror



4. Remove reference sphere; system aligned

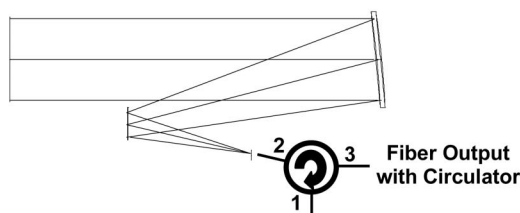


Fig. 3. Alignment procedure.

Table 2. Calibration Source Alignment Budget

Alignment 633 nm Mini-Fizeau Interferometer	Typical Wavefront Error (Single Pass) Optics and Alignment (λ rms)	Wavefront Error due to Alignment (Root-Sum-Square Out Optics) (λ rms)	Misalignment (Zemax Tolerancing)		
			x (μm)	y (μm)	z (μm)
$\lambda = 633$ nm					
Calibration optics: Step 1	0.032	0.021	8.4	8.4	8.4
Reference sphere: Step 2	0.012	0.011	≤ 0.1	≤ 0.1	≤ 0.1
Alignment with Circulator: Step 3	Power Returned (Submicrometer Resolution Ensures $>90\%$)		Micrometer Resolution (μm)		
Fiber feedback	91.8%		0.5	0.5	0.5
Stack-up (rounding up)			10	10	10
Fiber Cal Beam: Step 4	Single-Pass Wavefront Error due to Optics (Excludes Return Flat)	Wavefront Error due to Alignment (Zemax Prediction Based on Stack-Up)	Total Wavefront Error Prediction (Root-Sum-Square Value)		
$\lambda = 1550$ nm	0.0082λ rms	0.010λ rms	0.013λ rms		

the focus of the interferometer is located at the real focus of the OAP. Without moving the interferometer, the spherical reference mirror is inserted and aligned to it; i.e., the center of curvature of the spherical mirror is positioned at the focus of the interferometer, and thus the focus of the OAP. The optical fiber is then inserted in place of the interferometer and aligned to the transfer mirror using a five-axis positioning stage; fiber alignment is optimized via the power reflected back into the fiber, as monitored via port 3 of the circulator. When the power is maximized, the transfer mirror is removed and the fiber alignment to the OAP is complete. Note from Table 2 that the wavefront error due to the initial alignment of the OAP to the interferometer is 0.021λ rms at 633 nm, corresponding to 0.0086λ rms at 1550 nm. The final alignment error of the fiber to the OAP is calculated to be 0.010λ rms. This difference of 0.0014λ is within the resolution limit of the wavefront sensor used to characterize the system. The contribution of the fiber alignment to the wavefront error is negligible; within the limits of measurement, the interferometer alignment is transferred to the fiber.

The alignment budget in Table 2 shows how each alignment contributes to the final wavefront error. Each alignment step was modeled using the Zemax

software package to determine the amount of misalignment required to achieve either a specific wavefront error or a reflected power measurement. The final alignment was bounded based on the stack-up of the individual misalignments. A large beam splitter in the testbed optics (described in Section 3) is used as a return mirror for the interferometer alignment and is included in the wavefront error budget for Step 1 in Table 2; in subsequent steps, the wavefront error from this beam splitter was included in the budget for the testbed optics and does not contribute to the wavefront error of the calibration source.

To predict the wavefront error of the final calibration beam, several tolerance analyses were also performed using Zemax. Two systems were analyzed interferometrically: the OAP alignment and the transfer mirror alignment. The OAP alignment was modeled using a point source with an $F/5$ cone angle (5.7°). Perturbations were made in the x and z directions as indicated in Fig. 4. Similarly, the transfer mirror alignment to the fiber source was analyzed using the fiber-coupling feature in Zemax. This analysis provided a prediction of the returned power as a function of alignment and indicated that the critical alignment was the transverse direction (x). The theoretical predictions were confirmed experimentally using a test laser, a spherical mirror, and a circulator. Figure 5 shows the re-

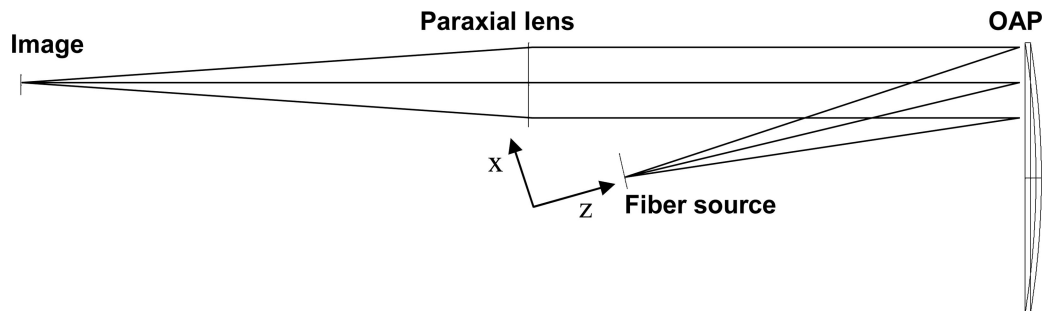


Fig. 4. Configuration for angular sensitivity analysis measurement.

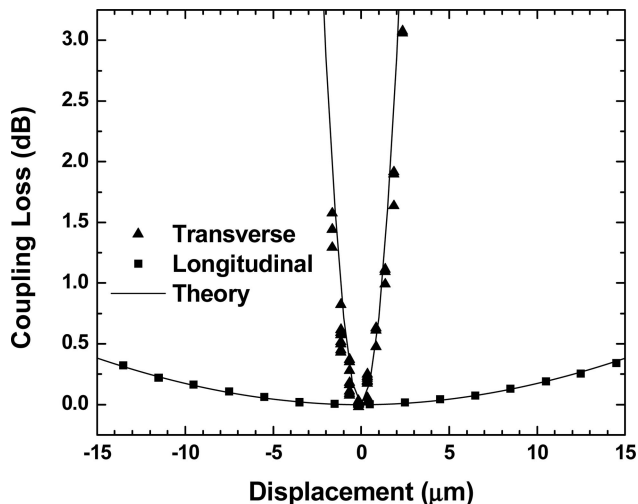


Fig. 5. Theoretical and measured fiber-retrosphere alignment sensitivity.

sults, which are in excellent agreement with the prediction. Stable coupling was achieved using commercial translation stages based on standard differential micrometers with $0.07 \mu\text{m}$ resolution.

3. Results

A. Wavefront Error

To determine the wavefront quality, the calibration beam was imaged through the optical testbed to a Shack-Hartman wavefront sensor, and wavefront data were generated using vendor-supplied reference files. The testbed consists of several high-quality optics, including a large turning mirror, a telescope that reduces the beam size, a lens relay, and several beam splitters. The testbed optics were all staked down with wrenches, pins, and/or epoxy to minimize alignment drift. In contrast, the calibration source is intended to be optimized on demand, and thus its optics are not permanently fixed. Based on test results for the individual testbed components, the wavefront error due to the testbed was estimated to be 0.0298λ rms at 1550 nm . Combined with the 0.013λ rms predicted wavefront error for the calibration source (see Table 2), the predicted performance for the combination of the calibration source and the testbed optics was 0.033λ rms. Upon initial alignment and optimization, performance of the combined system is often as good as 0.030λ rms, which is consistent with the prediction of 0.013λ rms for the calibration source. This corresponds to 0.065λ peak to valley or $<\lambda/15$.

The wavefront error of the combined calibration source and optical testbed was measured at 1545 nm over a 66 h period. Figure 6 shows the results, which exclude tilt but include all other aberrations. The data exhibits a clear temperature dependence of approximately $-0.15\lambda/^\circ\text{C}$; the facility is temperature controlled via an air handling system that operates with a 25–30 min cycle, resulting in the periodicity that is apparent in the data. The average value of the

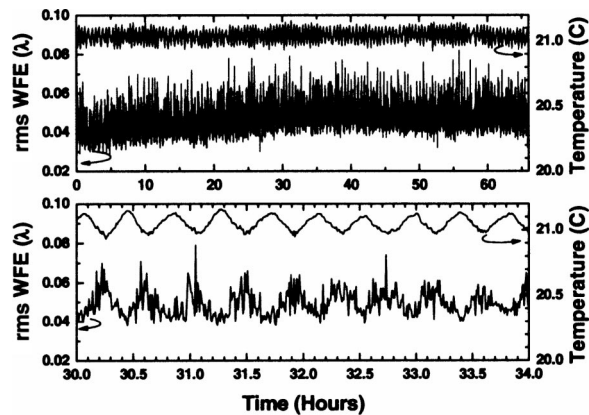


Fig. 6. rms wavefront error at 1545 nm and facility temperature.

wavefront error begins at $\sim 0.04\lambda$ rms and gradually increases to $\sim 0.05\lambda$ rms over a period of 30 h as the optical mounts settle. Beyond 30 h, the average value remains constant at $\sim 0.05\lambda$ rms. Both the long-term drift and the periodic variation are believed to be dominated by the mounts for the free-space optics in the calibration source.

B. Power Spectra and Dynamic Range

Power spectra for the calibration source are shown in Fig. 7 for three wavelengths that span the wavelength range. The three rows show power spectra at 20 mW, 200 mW, and 2.0 W, as confirmed by a National Institute of Standards and Technology traceable, free-space powermeter. The spectra were collected at the optical spectrum analyzer (OSA) tap point shown in Fig. 1. The length of fiber carrying the high-power signal beyond the tap point is less than 3 m, and nonlinearity-induced spectral distortion is negligible; thus the tap provides an accurate representation of the power spectrum launched into free space. As expected for a fiber-amplifier-based system, the performance at the middle wavelengths is excellent; at 1557 nm , the optical signal-to-noise ratio (OSNR) exceeds 44 dB in a 0.1 nm bandwidth at 2.0 W. Even at the edge wavelengths, where amplifier gain tilt causes preferential amplification of the suppressed modes of the master oscillator, the OSNR exceeds 31 dB. The optical power dynamic range is at least 20 dB at all wavelengths; maximum output power is limited to slightly more than 2 W by the rated damage threshold of the circulator.

C. Power Stability

Data from a long-term power stability measurement is shown in Fig. 8. After an initial warm-up period of $\sim 30 \text{ min}$, the amplifier was operated in a constant current mode to produce $\sim 1.45 \text{ W}$ of launched power at 1553 nm . As shown in Fig. 8, the power was stable to within 0.03 dB, or $<\pm 0.4\%$, over 24 h. Also shown in Fig. 8 are data from a temperature sensor located near the calibration source in the laboratory as well as a temperature sensor internal to

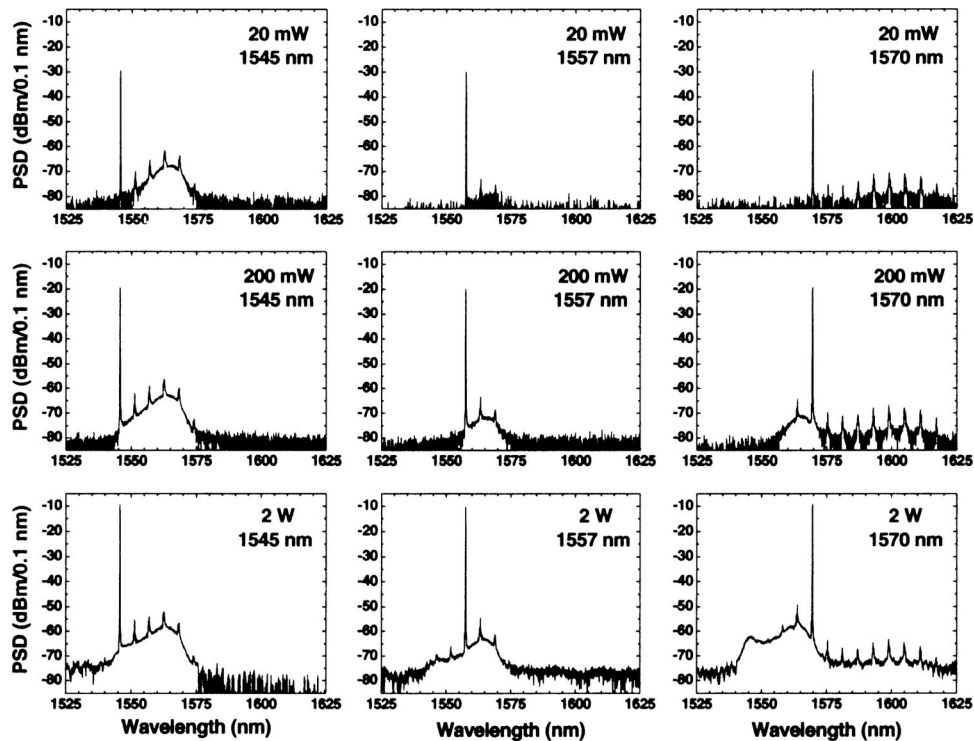


Fig. 7. Calibration source power spectra. PSD, power spectral density.

the optical amplifier. The periodicity of the residual variation in the calibration source output power reveals that the limiting factor for power stability is again the air-handling system of the facility: variation of the ambient temperature in the laboratory causes temperature fluctuations with the same periodicity inside the amplifier, and because the amplifier efficiency varies with temperature, the output power varies for a constant applied current.

D. Polarization Stability

Figure 9 shows the polarization in terms of orientation and ellipticity over the same 24 h period as Fig. 8. An arbitrary polarization state was selected at the

beginning of the test after the warm-up period by applying distinct voltages to each of the polarization-state generator's four actuators. The observed variation is $\leq \pm 1^\circ/\text{h}$ in orientation and $\leq \pm 0.02/\text{h}$ in ellipticity, limited by drift in the first few hours of the measurement. Because this initial drift is monotonic, we believe it to be caused by mechanical relaxation of the short length of single-mode fiber following the polarization state generator, which extends ~ 70 cm above the height of the optical table to the fiber launch positioner. The residual temperature variation in the facility has a minimal effect on polarization stability, manifesting itself as a slight periodic ripple in the data.

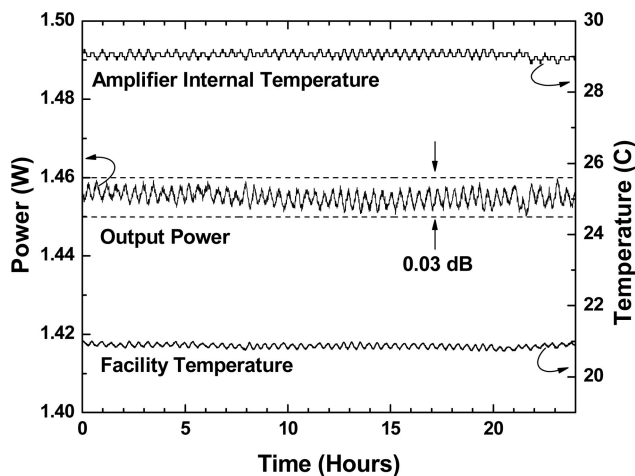


Fig. 8. Long-term power stability.

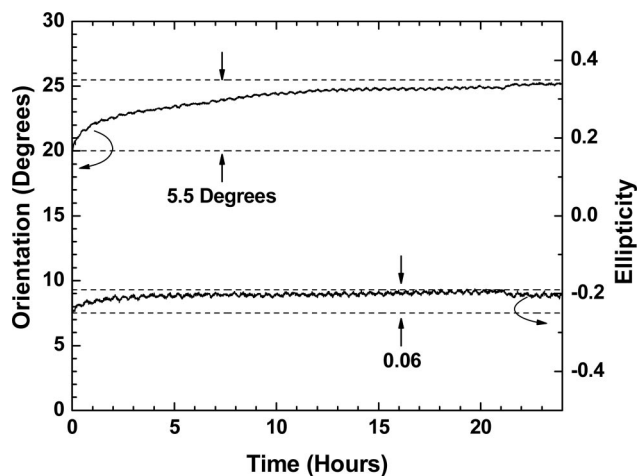


Fig. 9. Long-term polarization stability.

4. Summary

A 370 mm optical calibration source that is tunable from 1545 to 1570 nm and is stable in wavefront, power, and polarization has been demonstrated. By limiting the number of free-space optical components and utilizing the near-Gaussian mode of a single-mode optical fiber as the source, a wavefront better than 0.013λ rms has been achieved. The fiber-optic components allow the remoting of heat sources such as the optical amplifier to minimize thermal perturbations in the optical testing environment. Wavefront, power, and polarization stability are more than adequate to make accurate measurements on time scales from minutes to hours. Long-term wavefront and power stability are limited by residual thermal variation, while long-term polarization stability is limited by residual motion in the short length of single-mode fiber. Stability could be further enhanced using active thermal control or by using a power-stabilization control loop and an active polarization control loop via a tap in the free-space path. Likewise, the OSNR could be further enhanced by incorporating a tunable filter between the master oscillator and the fiber amplifier. The current implementation has only been exercised to ~ 2 W because of the power rating of the micro-optic circulator; however, similar components have been demonstrated to handle ~ 10 W with ~ 1 dB of insertion loss, and thus the output of the calibration source should readily scale to ~ 8 W.

The authors are grateful to several of their colleagues at MIT Lincoln Laboratory: Alan DeCew, Phil Chapnik, Kurt Abdelmaseh, Evan Stryjewski, Sarah Klein, and Tim Williams for optical support; John Peters, Bill Wilcox, and Cliff Williams for software support; and Colm Cryan and Peter Schulz for direction and useful comments. This work was sponsored by the Department of the Air Force under Air Force contract FA8721-05-C-0002. Opinions, interpretations, conclusions, and recommendations are those of the authors and are not necessarily endorsed by the United States Government.

References

1. M. C. Larson, Y. A. Akulova, C. Coldren, T. Lijeberg, G. A. Fish, S. Nakagawa, A. Dahl, P. Kozodoy, D. Bingo, M. Bai, N. Ramdas, S. Penniman, T. Wipiejewski, and L. A. Coldren, "High performance widely-tunable SG-DBR lasers," in *Novel In-Plane Semiconductor Lasers II*, C. F. Gmachl and D. P. Bour, eds., Proc. SPIE **4995**, 66–80 (2003).
2. S. Thaniyavarn, "Wavelength independent, optical damage immune Z-propagation LiNbO₃ waveguide polarization converter," *Appl. Physics Lett.* **47**, 674–676 (1985).
3. F. Heismann, "Integrated-optic polarization transformer for reset-free endless polarization control," *IEEE J. Quantum Electron.* **25**, 1989–1906 (1989).
4. T. H. Woods, "Highly reliable high power optical amplifiers at 1.55 μm ," in *Optoelectronic Integrated Circuits VIII*, L. A. Eldada and E. Lee, eds., Proc. SPIE **6124**, 61240Q1–9 (2006).
5. R. Noé, H. Heidrich, and D. Hoffmann, "Endless polarization control systems for coherent optics," *J. Lightwave Technol.* **6**, 1199–1207 (1988).